

Research on the Corrosion Behavior of 14Cr12Ni3Mo2VN Stainless Steel in a NaCl Solution with Different pH

Li Quan-de^{1,2,3}, Ran Dou^{1,3}, Zhai Fu-qiang⁴, Guo Wei-hua^{2,3}, Gao Zhen-huan^{2,3}, Gong Xiu-fang^{2,3}, Long Bin^{2,3}, Yang Ming^{2,3}, Ni Rong^{2,3}, Meng Hui-min^{1*}

¹ Institute of Advanced Materials and Technology, University of Science and Technology Beijing, Beijing 100083, China;

² State Key Laboratory of Long-life High Temperature Materials, Deyang 618000, China;

³ Dongfang Turbine Co.,Ltd., Deyang 618000, China;

⁴ Research Institute for New Materials Technology, Chongqing University of Arts and Sciences, Yongchuan Chongqing 402160, China;

*E-mail: menghm16@126.com

Received: 10 October 2019/ *Accepted:* 16 December 2019 / *Published:* 10 February 2020

Corrosion behaviors for 14Cr12Ni3Mo2VN martensitic stainless steels in chloride solutions with different pH values were investigated using an open circuit potential analysis, potentiodynamic polarization curve analysis, and Mott-Schottky analysis; furthermore, electrochemical impedance spectroscopy, scanning electron microscopy with energy dispersive spectroscopy and laser scanning confocal microscopy analyses were also conducted. The open circuit potential of the 14Cr12Ni3Mo2VN stainless steel in 100 mmol·L⁻¹ NaCl solution shifted from positive to negative with increasing pH, and the smallest electrochemical activity appeared at pH 9. With a reduction in the pH value from 9, the pitting potential and impedance value continuously decrease, and the main density N_d of the passivation film obviously increases. Additionally, the number of point defects inside the passivation film and the number of corrosion medium transmission channels increase. When the solution pH becomes alkaline, the passivation film of Cr has a strong tendency for hydroxylation and tends to exist in the form of hydroxide with poor protection, leading to a reduction in the corrosion resistance of the material. Fe, Cr, V and Mo in the corrosion pit selectively dissolve, which shows that Fe migrates to the solution in the form of ions, while Cr, V and Mo deposit in the pit in the form of oxides or hydroxides.

Keywords: pH value; Blades; Steam turbine; Electrochemistry; Corrosion

1. INTRODUCTION

The last two blade stages are an important part of a steam turbine for converting steam flow energy into useful work, producing much more than 10% of the total power output[1]. Blade failure

often causes the plant to be unable to operate normally, and the maintenance time and cost increase, which seriously affects the economic benefits of the plant[2-4]. In serious cases, blade failure can lead to damage of the whole stage impeller, or even can cause the scrapping of the whole steam turbine. Therefore, to improve the operational reliability of large power station equipment, it is necessary to solve the problem of blade failure, that is, improve the operational reliability of the blade[5-7].

To increase the safety of the steam turbine and prevent the corrosion of the last stage turbine blade, the concentration of impurities in the water is strictly controlled[8]. However, in the Wilson zone of a low-pressure cylinder (the dry and wet steam transfer area), the steam begins to condense into liquid water, and impurities in the steam are redistributed. Ammonia, an alkalizing agent with a large distribution coefficient, mainly exists in the vapor phase[9,10]. Acidic gas and organic acid (such as acetic and formic acid) in the steam prefer distributing in the initial water setting to reduce the pH value of the aqueous phase so that the part of the passivation film on the blade surface is destroyed and exposed to the active substrate; the above results in the formation of a corrosion battery with the passivation surface and brings the risk of pitting[11,12]. A certain amount of NaOH is added to the boiler water to increase the pH value of the initial condensation and reduce the amount of ammonia, which is widely used in power plant operation, but the pH value of the condensed water is also increased by the addition of NaOH[13,14].

At present, research on the corrosion behavior of turbine blades at the last stage has mainly focused on speculating corrosion factors (such as Cl^- in condensing water and dissolved oxygen) and the corrosion process of corroded blades[6,9,11,12]. However, the influence of the pH value in the condensing water on the corrosion behavior of turbine blades has rarely been reported[15,16]. Therefore, it is necessary for the safe operation of steam turbines to study the influence of pH value on its blade corrosion behavior. Herein, the exact corrosion behaviors of 14Cr12Ni3Mo2VN martensitic stainless steel were investigated, and the related corrosion mechanism was discussed. The experimental results can provide a theoretical basis and data support for the operation and development of a practical steam turbine and the choice of blade material.

2. EXPERIMENTAL

2.1 Working electrode preparation

14Cr12Ni3Mo2VN martensitic stainless steel was used as the base material in this work. The chemical composition in mass percent is 0.15% C, 11.50% Cr, 1.61% Mo, 0.75% Mn, 0.12% Si, 2.97% Ni, 0.073% S, 0.013% P, 0.28% V, 0.034% N and Fe as the balance.

2.2 Experimental

In the sample preparation stage, after cutting 10 mm×10 mm×10 mm specimens, they were cold-mounted by an epoxy resin to prevent crevice corrosion, and a 1 cm² exposed area was used as a working electrode. Prior to the electrochemical setup experiment, the specimens were polished to a

mirror-like finish with a grinding machine, washed in distilled water, and then eventually dried by hot air. For electrochemical measurements, a three-electrode setup consisting of a specimen as the working electrode, a saturated calomel electrode (SCE) as the reference electrode, and a platinum plate as the counter electrode was used. The experimental electrochemical medium was a NaCl solution ($100 \text{ mmol}\cdot\text{L}^{-1}$), whose pH value was adjusted to 2, 5, 7, 9 and 12 by using hydrochloric acid and sodium hydroxide solutions.

APARSTAT4000 electrochemical workstation was used to perform the electrochemical measurements. Before the electrochemical tests, the working electrode was immersed in a test solution injected with 99.999% argon for 72 h. First, the open circuit potential (OCP vs. SCE) changes with time were recorded for 30 min until they were stable. Then, electrochemical impedance spectroscopy (EIS) experiments were conducted at the OCP with a voltage perturbation amplitude of 10 mV in a frequency range of 10 kHz to 0.01 Hz. The potentiodynamic measurement rate was set to $1 \text{ mV}\cdot\text{s}^{-1}$ and the scanning range was from -800 mV (vs. SCE) to the anodic potential value. When the anodic polarization current density reached $1 \text{ mA}\cdot\text{cm}^{-2}$, reverse scanning was immediately carried out until intersecting with the anodic polarization curve and then stopped. ZSimpWin software was used for an EIS data fitting analysis. A Mott-Schottky measurement was taken between -0.5 and 1.2 V (vs. SCE) with an ac signal amplitude of 10 mV. The test frequency was at 1 kHz, and each parallel sample was tested at least 3 times for all of the above measurements.

After testing, the samples were rinsed with ethanol and deionized water and dried with cold air. The corrosion micromorphology of the working electrode surface was observed by a Thermo Fisher APREO scanning electron microscope (SEM) and an OLYMPUS OLS5000 laser scanning confocal microscope (LSCM); additionally, the composition was measured by energy dispersive spectroscopy (EDS).

3. RESULTS AND DISCUSSION

3.1 Open circuit potentials

The open circuit potentials of the 14Cr12Ni3Mo2VN martensitic stainless steel samples in NaCl solutions with different pH values are shown in Fig. 1. The open circuit potential of 14Cr12Ni3Mo2VN stainless steel shifted from -0.374 V (pH 2) to -0.104 V with increasing pH values, and the most positive potential was obtained with pH 9. As we know, the more negative the open circuit potential is, the greater the occurrence of corrosion [17,18]. It can be seen that the electrochemical activity of the 14Cr12Ni3Mo2VN stainless steel decreases at the beginning and then increases with increasing pH, which may be due to a competitive adsorption of OH^- on the electrode surface in the solution and changes in the passive film composition [19].

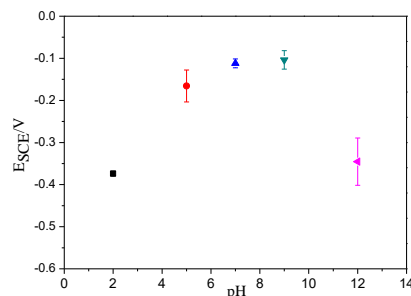


Figure 1. Open circuit potentials for the 14Cr12Ni3Mo2VN martensitic stainless steel in solutions with different pH values.

3.2 Potentiodynamic polarization

The potentiodynamic polarization curves of 14Cr12Ni3Mo2VN samples in solutions with different pH values are shown in Fig. 2. The corrosion potential (E_{corr}) and corrosion current (I_{corr}) are shown in Table 1. The potential value corresponding to the current density rapidly increasing to $100 \mu A \cdot cm^{-2}$ on the polarization curve was due to the pitting potential (E_{pit} , see Table 1). All slopes for the cathodic polarization curves in Fig. 2 are very close, indicating that there is no obvious effect of pH value on the cathodic polarization rate of the 14Cr12Ni3Mo2VN stainless steel and that the value of pH mainly affects the anodic process [20]. When the pH was 5, 7 and 9, the pitting potential of the 14Cr12Ni3Mo2VN samples was 0.235 V, 0.248 V and 0.307 V, respectively, which may be induced by a competitive adsorption between Cl^- and OH^- on the electrode surface and the change from Cl^- to OH^- being dominant as the pH value increased, leading to a more protective passivation film on the surface of the working electrode [21,22]. Regardless of a decrease or increase in the solution pH value (from pH 9), the pitting and protection potential of the 14Cr12Ni3Mo2VN samples show a decreasing trend (Fig. 2). The self-repairing ability of the passivation film becomes weak, and the pitting sensitivity increases, resulting in the corrosion resistance of the passivation film also decreasing [23,24].

When the pH value increases to 12, the pitting potential as defined above increases rapidly, which is inconsistent with the corrosion resistance in the open circuit potential test. This may be because the pH value is too high, thus, the oxygen evolution process is superior to the pitting reaction that occurs on the electrode surface. The oxygen evolution reaction takes place before the pitting process and has a certain lag effect associated with it, which leads to the phenomenon of a high pitting potential in the polarization curve of kinetic potential. In addition, Fe compounds in the passivation film at high pH (pH 12) are more stable than Cr and Mo compounds, and the passivation film is mainly composed of these less protective Fe compounds, leading to a decrease in the corrosion resistance of the working electrode [21]. However, the hysteresis ring and peak current density of the dynamic potential polarization curve during the reverse scan indicate that pitting erosion occurred at the stage of a positive potential sweep. The corrosion potential in Fig. 2 is more negative than the open circuit

potential in Fig. 1, which is caused by the cathode polarization of the sample in the electrochemical polarization test.

A peak current density and hysteresis ring appear in the reverse scans of the dynamic potential polarization curves at different pH values, except at pH 2. For the reverse scan potentials, the current density does not immediately decrease, as there was a section where it increased before starting to decrease. This is because the passivated film on the surface of the work electrode was broken down in forward scanning, which leads to pitting corrosion occurring on the surface of the sample[25]. A blocking effect forms due to the accumulation of corrosion products in the corrosion holes of the anode; the above results in improving the concentration of metal cations in the occlusion area. To maintain electrical neutrality in the corrosion pit, Cl^- moves from the outside to the inside of the corrosion pit. As a result, the concentration of Cl^- in the hole constantly increases. Due to the high conductivity of a concentrated salt solution, the internal resistance of the occluded battery is very low, and the corrosion is ongoing[26,27]. At the same time, diffusion is difficult, and the solubility of oxygen is very low, leading to the development of pitting corrosion and hindering metal repurification. Even the reverse scan in the negative potential direction could not immediately prevent the further expansion of pitting corrosion, resulting in a continuous increase of current density[28].

The peak current density appears in the dynamic potential polarization curves of the reverse scan in a pH 2 solution, but no obvious hysteresis ring appears, which may be because the H^+ concentration in solution is high and there is a large number of formed corrosion pits (Fig. 6a) and shallow on the electrode surface to make it difficult to form blocking corrosion holes. When the reverse scan potential reaches the negative side, the further expansion of pitting corrosion can be stopped immediately. However, each reverse scan curve intersects the forward scan curve at a certain potential, and then the current density remains lower than that of the forward scan, indicating that a protective passivation film can be formed on the surface of each sample at this time. However, the protection potential shifts from positive to negative with increasing pH, and the most positive protection potential of the sample is obtained with pH 9, indicating the increasing difficulty of repairing the corroded passivation film[29].

Usually, in neutral or alkaline solutions, the higher the pH, the more stable the Fe oxide and the thicker the passivation film. In acidic solution, the oxidation rate of Cr is lower than that of Fe. With a decrease in the pH value, the Fe content in the passivation film decreases, but the Cr content increases. With the change of pH value, the passivation film will be selectively dissolved, and its composition and properties will be changed accordingly. In weak acid and weak alkaline environments, Cr exists in the form of dense oxides of Cr_2O_3 , and the formed passivation film formed has the greatest resistance to the diffusion of corrosive ions. Therefore, the passivation film has the best corrosion resistance in the above pH range.

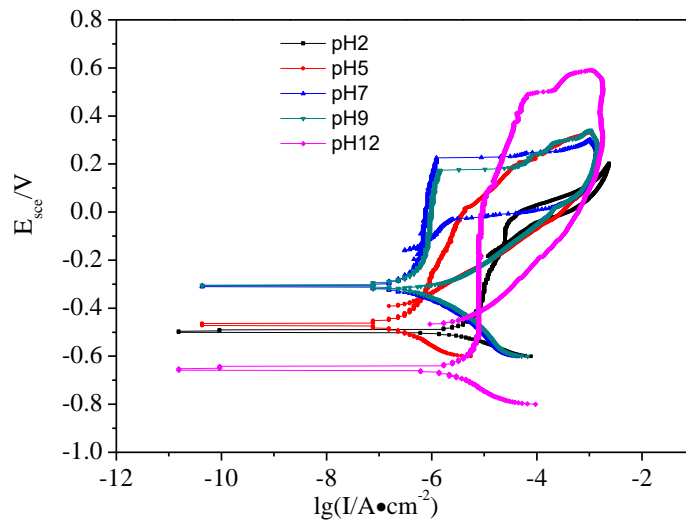


Figure 2. Potentiodynamic polarization curves of the 14Cr12Ni3Mo2VN samples in solutions with different pH values.

Table 1. Electrochemical Parameters of the 14Cr12Ni3Mo2VN samples with different pH values

pH value	E_{corr}/V	$I_{corr}/(\mu A \cdot cm^{-2})$	E_{pit}/V
2	-0.491	2.269	0.028
5	-0.464	0.158	0.235
7	-0.351	0.258	0.248
9	-0.341	0.167	0.307
12	-0.648	2.234	0.498

3.3 Electrochemical impedance spectroscopy

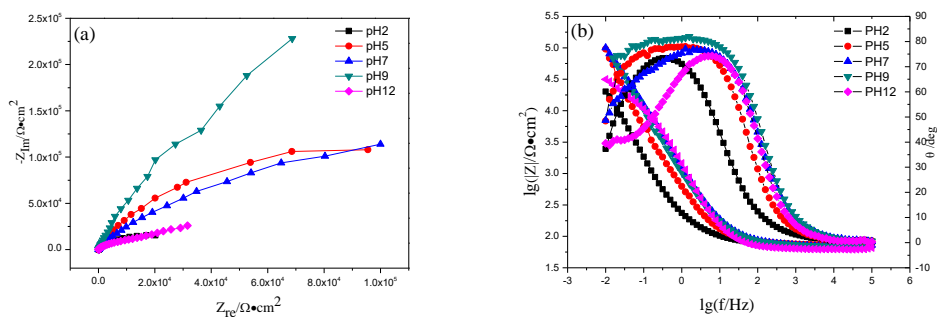


Figure 3. Electrochemical impedance spectroscopy of the 14Cr12Ni3Mo2VN martensitic stainless steel samples in solutions with different pH values: (a)Nyquist and(b)Bode plots.

The electrochemical impedance spectroscopy test results of the 14Cr12Ni3Mo2VN samples in solutions with different pH values are shown in Fig. 3. The impedance of each system changes with various pH values, indicating that the passivation film protection on the surface of the sample becomes

better or worse and that the corrosion rate and resistance shifts from positive to negative with increasing pH values[30].

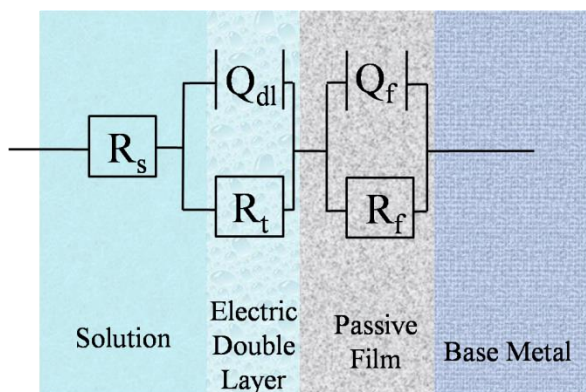


Figure 4. Equivalent circuit model fitted from the electrochemical impedance spectroscopy results.

The electrochemical impedance spectroscopy for solutions at different pH values were analyzed by the equivalent circuit shown in Fig. 4 (see Table 2) [31]. Among them, R_s is the solution resistance, $CPE(Q_f)$ is the passivation film capacitance, and R_f is the passivation film resistance. $CPE(Q_{dl})$ and R_t are the capacitance and charge transfer resistance of the surface double layer, respectively. $CPE(Q)$ is generally used for the uniform distribution of current on the stainless steel surface and the high surface roughness. The impedance value can be calculated by the following formula:

$$Z_Q = (j\omega)^{-n}/Y_0 \quad (1)$$

where Y_0 is the admittance modulus of the CPE, ω is the angular frequency, n is the diffusion exponent of the CPE, whose range in value is set to $0 \leq n \leq 1$. When $n=0.5$, the CPE is considered the Warburg impedance. When $n=1$, it is considered to be the ideal capacitance; when $0.5 < n < 1$, CPE is in a middle state between the above-mentioned states. As shown in Table 2, the R_{tmax} of the 14Cr12Ni3Mo2VN sample is $9.67 \times 10^5 \Omega \cdot cm^2$, which is the tendency in a $100 \text{ mmol} \cdot L^{-1} NaCl$ solution at pH 9. When the pH value increases or decreases from 9, the R_f gradually decreases, which indicates that the passivation film impedance decreases and reduces the corrosion protection[32,33]. The corrosion resistance fitted by the equivalent circuit has good consistency with the open circuit potential and potentiodynamic polarization test results.

Table 2. Parameters of the equivalent circuit

pH value	$R_s/(\Omega \cdot cm^2)$	Q_{dl}		$R_t/(\Omega \cdot cm^2)$	Q_f		$R_f/(\Omega \cdot cm^2)$
		$Y_0/(\Omega^{-1} \cdot cm^{-2} \cdot S^{n1})$	n_1		$Y_0/(\Omega^{-1} \cdot cm^{-2} \cdot S^{n2})$	n_2	
2	68.15	2.46×10^{-3}	0.55	22.4	2.80×10^{-4}	0.87	3.75×10^4
5	73.82	1.97×10^{-4}	0.81	0.77×10^4	8.54×10^{-5}	0.98	2.41×10^5
7	70.02	6.40×10^{-5}	0.89	3.09×10^5	4.45×10^{-5}	0.85	2.62×10^5
9	70.35	8.41×10^{-5}	0.83	1.74×10^4	3.46×10^{-5}	0.97	9.67×10^5
12	58.97	4.93×10^{-5}	0.98	8.39×10^5	1.13×10^{-4}	0.85	4.14×10^4

3.4 Mott-Schottky analysis

When Cl^- exists in the solution, it will compete with OH^- in adsorbing on the surface of the stainless steel sample. Further increasing the pH value will result in more OH^- adsorption on the electrode surface, changing the corrosion behavior of the stainless steel sample[21]. Usually, the passivation film formed on the surface of a metal or alloy has semiconductor properties[34,35]. When the passivation film contacts the solution, a space charge layer will be formed on the side of the passivation film, and a Helmholtz layer will be formed on the side of the solution[36]. At this time, the solution and the semiconductor film carry an opposite charge, and the excess charge of the semiconductor film will be distributed in the space charge layer[37,38]. When the space charge layer is in a depleted state, the capacitance of the space charge layer and the measured electrode potential can be described and analyzed by the Mott-Schottky equation[39].

The space charge capacitance has the following relationship with the measured potential:

$$\frac{1}{C^2} = \frac{2}{\varepsilon\varepsilon_0 e N_d A^2} \left(E - E_{fb} - \frac{kT}{e} \right) \quad (2)$$

$$\frac{1}{C^2} = -\frac{2}{\varepsilon\varepsilon_0 e N_a A^2} \left(E - E_{fb} - \frac{kT}{e} \right) \quad (3)$$

$$W = \left[\frac{2\varepsilon\varepsilon_0}{e N_d} \left(E - E_{fb} - \frac{kT}{e} \right) \right]^{\frac{1}{2}} \quad (4)$$

where C is the space charge layer capacitance of the passivation film, F; E is the scanning potential, V; E_{fb} is the flat band potential, V; ε_0 is the vacuum dielectric constant, $8.85 \times 10^{-14} \text{ F} \cdot \text{cm}^{-1}$; ε is the relative dielectric constant at 15.6; N_D and N_A represent the donor and acceptor densities for n-type and p-type semiconductors, respectively, cm^{-3} ; A represents the sample area, which is set to 1 in this paper, cm^2 ; K is the Boltzmann constant, $1.38 \times 10^{-23} \text{ J} \cdot \text{K}^{-1}$; e is the electron charge, $1.6 \times 10^{-19} \text{ C}$; T shows the thermodynamic temperature, K; and W is the thickness of the passivation film, 10^{-10} m . Equation (2) represents n-type semiconductor characteristics of the passivation film, while Equation (3) shows those of a p-type. Equation (4) represents the thickness of the passivation layer.

Fig. 5 shows the Mott-Schottky curve of the stainless steel samples in solutions with different pH values. It can be seen that the Mott-Schottky curve has roughly the same variation trend with 2 intervals[40]. The slope of the fitted straight line is positive, showing an n-type semiconductor. The second interval, in which the slope is negative, presents characteristics of a p-type semiconductor. The main density of N_d is one of the important parameters to describe the passivation properties of the stainless steel samples. Table 3 shows the N_d value calculated by fitting the Mott-Schottky curve (Equation (2)). With increasing pH, the main density N_d of the passivation film donor decreases at first and then increases significantly[41,42].

Whether reducing or increasing the pH value from pH 9, the point defects in the passivation film increase, and the corrosion medium transfer channels increase. Furthermore, the charge transfer resistance decreases, which makes the charge transfer and electrode reaction easier. According to Equation (4), when N_d increases, the thickness of the passivation film W decreases and the stability of the passivation film becomes worse, showing that its corrosion resistance decreases; the above indicates that with a decrease in pH value from pH 9, the point defects of the passivation film on the surface increase, resulting from forming more channels conducive to Cl^- transfer and promoting its adsorption on the surface of the stainless steel matrix, which further increases the active points on the

surface that promote pitting. When the pH value becomes more alkaline, the main density N_d of the passive film donor increases, which is due to more OH^- competing for adsorption on the surface of the sample electrode. Although the adsorption of Cl^- on the electrode surface is inhibited, the passivation film of Cr has a strong tendency of hydroxylation and tends to exist in the form of a hydroxide with poor protection, leading to a reduced corrosion resistance of the material[21].

According to the above results, the competitive adsorption between the Cl^- and OH^- ions on the surface of the 14Cr12Ni3Mo2VN samples can increase the point defect density and reduce the thickness and stability of the passivation film, which accelerates the occurrence of corrosion[43]and is consistent with the electrochemical impedance spectroscopy results.

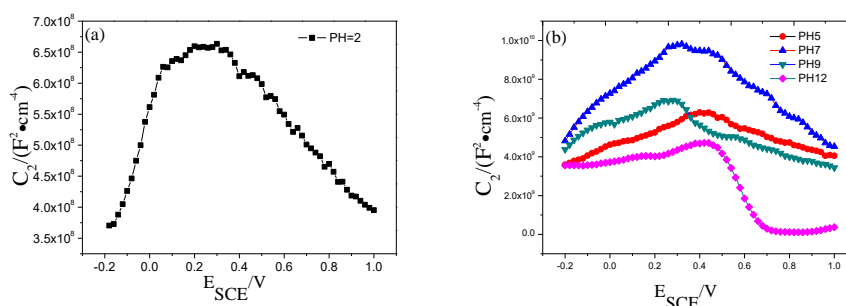


Figure 5. Mott-Schottky curves of the 14Cr12Ni3Mo2VN samples in solutions with different pH values (a) pH 2,(b) pH 5, pH 7, pH 9,and pH 12.

Table 3. Donor current density

pH value	$N_d/(10^{21} \text{ cm}^{-3})$
2	7.13
5	1.88
7	1.72
9	1.06
12	2.24

3.5 Morphology and composition analyses

The etched pit morphology results are shown in Fig. 6 and Fig. 7. In the solution with a pH 2, the 14Cr12Ni3Mo2VN stainless steel produces more corrosion pits with a diameter of approximately 30 μm (Fig. 6a and Fig.7a), which may be due to a high concentration of H^+ in the solution and more active spots on the surface of the working electrode;the above makes the sample more conducive to the formation of pits.In the solution with a pH 5 or 7, the number of pits on the surface of the working electrode decrease significantly, and the diameter of the pits increase to 100 μm (Fig. 6b, 6c, 7b, 7c). This may be due to the increasing pH value of the solution; thus, the corrosion resistance of the surface passivation film becomes better, and the number of pits is inhibited.There is no significant increase in the number of pits at pH 9, and the diameter of the pits decreases to approximately 50 μm (Fig. 6d, 7d).However, when the pH increases to 12, the size of the corrosion pit increases rapidly to more than 130 μm (pH 12, Fig. 6e, 7e), and the morphology is more complex [44], which is mainly due to the poor corrosion resistance of the passivation film in a strong alkaline solution.

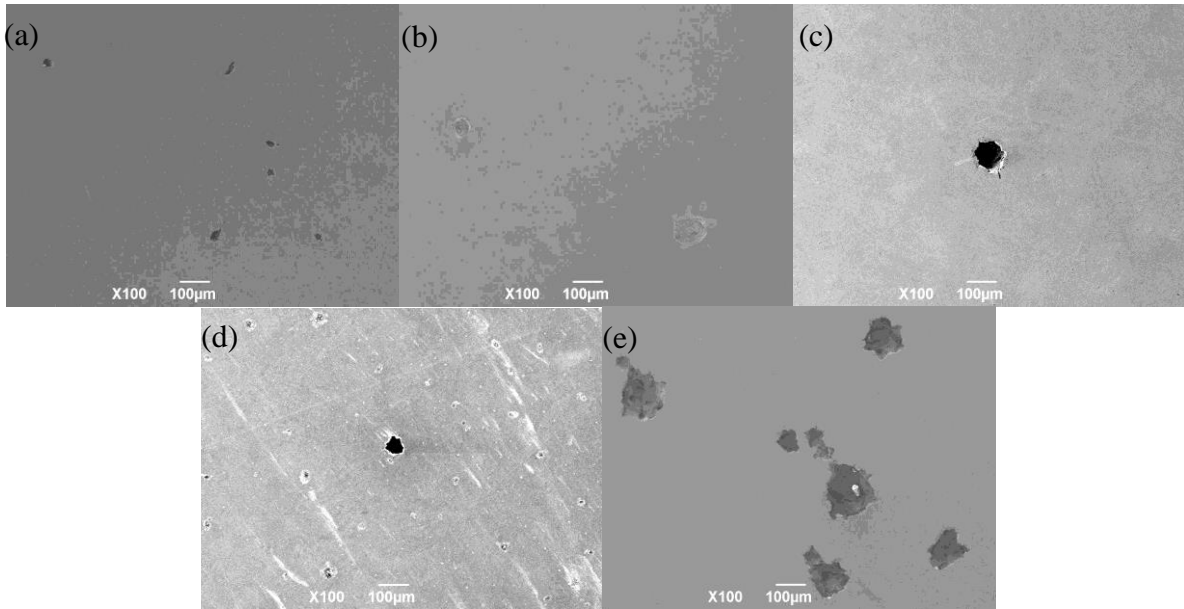
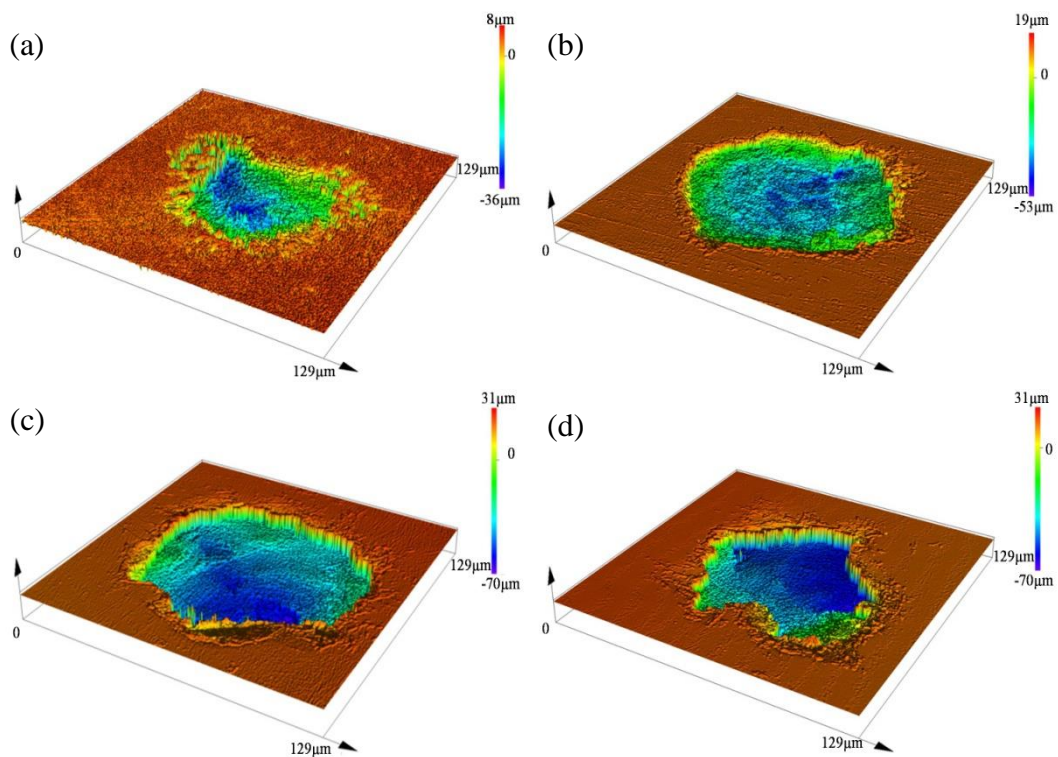


Figure 6. Pit morphologies(SEM) of 14Cr12Ni3Mo2VN in solutions with different pH values:(a) pH 2,(b) pH 5,(c) pH 7,(d) pH 9,and (e) pH 12.

Typical corrosion pits on the sample surfaces were selected and marked as being either the pit interior or the substrate. An energy dispersive spectroscopy (EDS) analysis was conducted on the selected areas (Fig. 8), and the results are shown in Table 4. According to the EDS analysis results, the corrosion products are mainly composed of Fe,Cr,V and Mo[45]. Corrosion products in the pits are mainly composed of Cr,V and Mo.



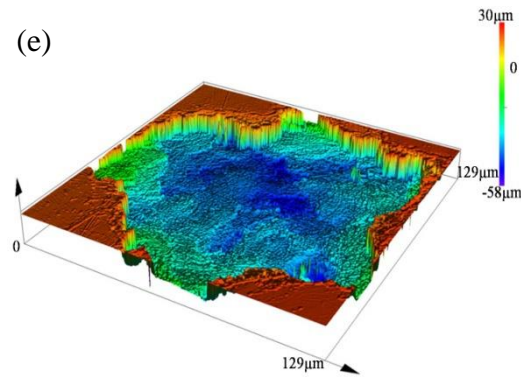
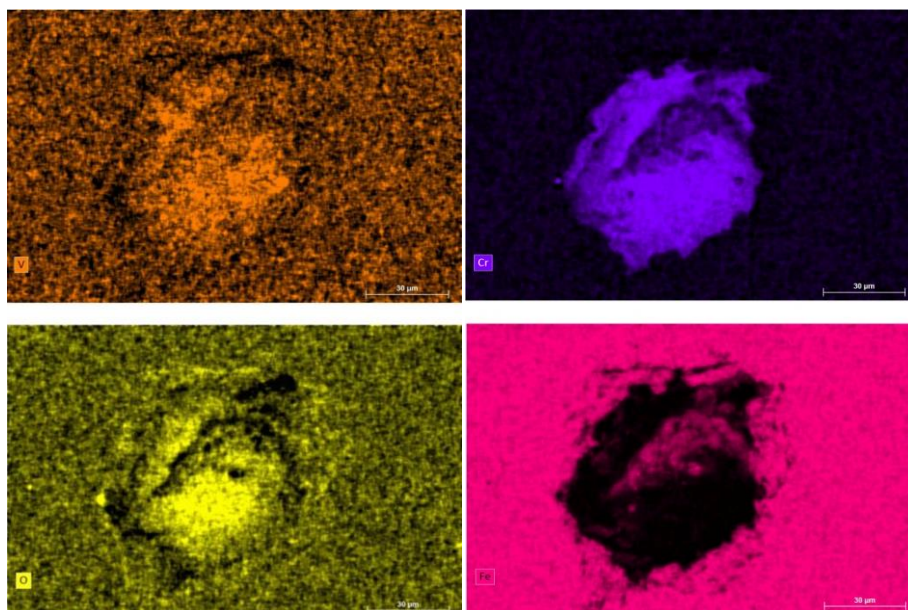


Figure 7. Pit morphologies (LSCM) of the 14Cr12Ni3Mo2VN martensitic stainless steel samples in solutions with different pH values: (a) pH 2, (b) pH 5, (c) pH 7, (d) pH 9, and (e) pH 12.

The content of Cr, V and Mo of the corrosion products inside the pits is higher than that of the corrosion products on the outside, but the Fe content is completely opposite compared with those of Cr, V and Mo, indicating that when pitting corrosion occurs on the surface and spreads inward, Fe, Cr, V and Mo undergo selective dissolution. Fe quickly migrates out of the corrosion pit, while Cr, V and Mo slowly migrate and deposit inside the pit to a certain extent; the above results in a high Cr, V and Mo content in the pit interior and an aggregation of Fe outside of the pit area [46-49]. In addition, the O content in the corrosion pit is much higher than that in other areas, indicating that Cr, V and Mo oxides or hydroxides exist in the corrosion products. That is, during the corrosion of stainless steel, Fe is dissolved into the medium in the form of ions, while Cr, V and Mo are deposited in the form of oxides or hydroxides [50,51].



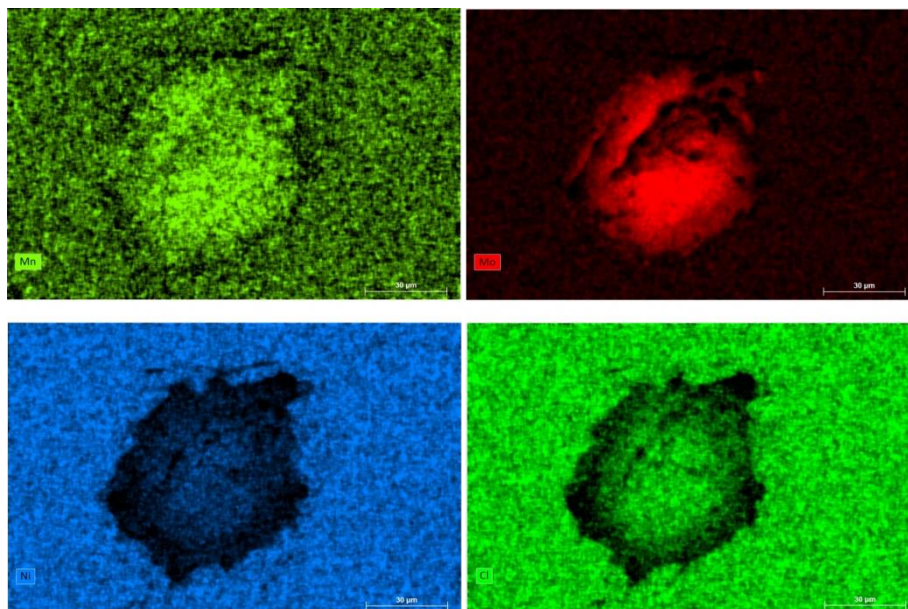


Figure 8. EDS spectra of the pits in the 14Cr12Ni3Mo2VN martensitic stainless steel samples.

Table 4. EDS analysis of the pit interior and substrate

Element	Fe	Cr	O	Ni	Mo	Mn	V	Cl
Pit interior(at%)	39.72	26.99	15.69	2.02	12.82	0.69	1.82	0.29
Substrate(at%)	76.17	9.97	7.10	4.70	1.23	0.62	0.18	0.02

4. CONCLUSIONS

The open circuit potential of the 14Cr12Ni3Mo2VN stainless steel shifted from positive to negative with an increasing pH value of the solution, and the most positive potential was obtained at pH 9.

With decreasing pH values from pH 9, the point defects of the passivation film on the surface increase, forming more channels conducive to Cl⁻ transfer and promoting its adsorption on the surface of the stainless steel matrix; the above further increases the number of active points on the surface to promote pitting.

When the solution pH becomes more alkaline, the passivation film of Cr has a strong tendency toward hydroxylation and tends to exist in the form of a hydroxide with poor protection, leading to a reduced corrosion resistance of the material even though the adsorption of Cl⁻ on the electrode surface is inhibited.

When pitting corrosion occurs on the surface and spreads into the pits, Fe,Cr,V and Mo undergo selective dissolution;Fe migrates out of the pit in the form of ions, while Cr,V and Mo are deposited in the form of oxides or hydroxides in the pit.

ACKNOWLEDGMENTS

This work is financially supported by the fund of the State Key Laboratory of Long-life High Temperature Materials(No.DTCC28EE190230) and the Sichuan Applied Foundation Project(No. 2019YJ0699).

References

1. Sławomir Dykas, Mirosław Majkut, Krystian Smółka, Michał Strozik, *Int. J. Heat.Mass Tran.*, 120 (2018) 9.
2. C.R.F. Azevedo, A. Sinátoro, *Eng. Fai. Anal.*, 16 (2009) 2290.
3. D.G. Hattingh, M.N. James, M. Newby, R. Scheepers, P. Doubell, *Theor.Appl.Fract.Mec.*, 83 (2016) 125.
4. Jolanta Baran, *Energ, Convers, Manage.*, 116 (2016) 18.
5. A. Ahmadpour, S.M.A. Noori Rahim Abadi, J.P. Meyer, *Energy*, 119 (2017) 675.
6. Sanjeev Saxena, J.P. Pandey, Ranjit Singh Solanki, Gaurav K. Gupta, O.P. Modi, *Eng. Fai. Anal.*, 52 (2015) 35.
7. S. Cano, J.A. Rodriguez, J.M. Rodriguez, J.C. Garcia, F.Z. Sierra, S.R. Casolco, M. Herrera, *Eng. Fai. Anal.*, 97 (2019) 579.
8. J.A. Rodríguez, L. Castro, A.L. Tejada, J.C. García, J.M. Rodríguez, E. Galindo, Y. El Hamzaouic, *Eng. Fai. Anal.*, 104 (2019) 39.
9. Marko Katinić, Dražan Kozak, Ivan Gelo, Darko Damjanović, *Eng. Fai. Anal.*, 106 (2019) 104136
10. Xu Han, Wei Zeng, Zhonghe Han, *Appl. Therm. Eng.*, 164 (2020) 114538.
11. M. Nurbanasari, Abdurrachim, *Case. Stud. Eng. Fail. Anal.*, 2 (2014) 54.
12. Ernst Plesiutchnig, Patrick Fritzl, Norbert Enzinger, Christof Sommitsch, *Case. Stud. Eng. Fail. Anal.*, 5–6 (2016) 39.
13. Akash Shukla, S.P. Harsha, *Mater.Today.*, 2(2015) 2056.
14. Loveleen Kumar Bhagi, Vikas Rastogi, Pardeep Gupta, Swastik Pradhan, *Mater.Today.*, 5(2018) 28117.
15. Goutam Das, Sandip Ghosh Chowdhury, Ashok Kumar Ray, Swapan Kumar Das, Deepak Kumar Bhattacharya, *Eng. Fail. Anal.*, 10 (2003) 85.
16. A.P. Tschiptschin, C.R.F. Azevedo, *Eng. Fail. Anal.*, 12 (2005) 49.
17. Farzin Arjmand, Lefu Zhang, Jiamei Wang, *Nucl. Eng. Dign.*, 322 (2017) 215.
18. Karthikeyan Selvam, Jaskaran Saini, Gopinath Perumal, Aditya Ayyagari, Riyadh Salloom, Riya Mondal, Sundeep Mukherjee, Harpreet Singh Grewal, Harpreet Singh Arora, *Tribol. Int.*, 134 (2019) 77.
19. C.J. Scheuer, F.A.A. Possoli, P.C. Borges, R.P. Cardoso, S.F. Brunatto, *Electrochim. Acta*, 317 (2019) 70.
20. Xudong Chen, Yusheng Li, Yuntian Zhu, Yakui Bai, Bin Yang, *Appl. Surf. Sci.*, 481 (2019) 1305.
21. Arash Azimi Dastgerdi, Andrea Brenna, Marco Ormellese, MariaPia Peddeferri, Fabio Bolzoni, , *Corros. Sci.*, 159 (2019) 108160.
22. Thunyaluk Pojtanabuntoeng, Mobin Salasi, *Electrochim. Acta.*, 258 (2017) 442.
23. D.G. Li, J.D. Wang, D.R. Chen, P. Liang, *J. Power Sources.*, 272 (2014) 448.
24. L. Li, C.F. Dong, K. Xiao, J.Z. Yao, X.G. Li, *Cons. Build. Mater.*, 68 (2014) 709.
25. I.G. Ogunsanya, C.M. Hansson, *Materialia*, 6 (2019) 100321.
26. G. Tranchida, M. Clesi, F. Di Franco, F. Di Quarto, M. Santamaria, *Electrochim. Acta.*, 273 (2018) 412.
27. J. Li, C.W. Du, Z.Y. Liu, X.G. Li, M. Liu, *Constr. Build. Mater.*, 189 (2018) 1286.
28. Xuanpeng Li, Yang Zhao, Wenlong Qi, Junfeng Xie, Jidong Wang, Bin Liu, Guanxin Zeng, Tao Zhang, Fuhui Wang, *Appl. Surf. Sci.*, 469 (2019) 146.

29. M.J.K. Lodhi, K.M. Deen, M.C. Greenlee-Wacker, Waseem Haider, *Addit. Manuf.*, 27 (2019) 8.
30. Fenfen Yang, Huijun Kang, Enyu Guo, Rengeng Li, Zongning Chen, Yanhua Zeng, Tongmin Wang, *Corros. Sci.*, 139 (2018) 333.
31. Hong Luo, Qiang Yu, Chaofang Dong, Gang Sha, Zhenbao Liu, Jianxiong Liang, Li Wang, Gang Han, Xiaogang Li, *Corros. Sci.*, 139 (2018) 185.
32. Odhiambo John Gerald, Li WenGe, Li Zhang, Zhao YuanTao, Li Cheng Lon, *Mater. Chem. Phys.*, 239 (2020) 122010.
33. L. Pan, C.T. Kwok, K.H. Lo, *J. Mater. Process. Tech.*, 277 (2020) 116448.
34. J. Izquierdo, L. Martín-Ruíz, B.M. Fernández-Pérez, R. Rodríguez-Raposo, J.J. Santana, R.M. Souto, *Electroanal. Chem.*, 728 (2014) 148.
35. Zhenwei Yan, Xianjie Yuan, Zhaojun Tan, Mingqi Tang, Zaiqiang Feng, *Int. J. Electrochem. Sc.*, 13(2018)353.
36. Ibrahim M. Gadala, Akram Alfantazi, *Appl. Surf. Sci.*, 357 (2015) 356.
37. Lv Jinlong, Huijin Jin, Liang Tongxiang, *Mater. Lett.*, 256 (2019)126640.
38. Tigang Duan, Wenshan Peng, Kangkang Ding, Weimin Guo, Jian Hou, Wenhua Cheng, Shaotong Liu, Likun Xu, *Ocean. Eng.*, 189 (2019) 106.
39. A. Fattah-alhosseini, S. Vafaeian, *J. Alloy. Compd.*, 639 (2015) 301.
40. Alberto Adan Mas, Teresa M. Silva, Liliane Guerlou-Demourgues, Maria Fatima Montemor, *Electrochim. Acta.*, 289 (2018) 47.
41. Sabrina Marcelin, Benoit Ter-Ovanessian, Bernard Normand, *Electrochem. Commun.*, 66 (2016) 62.
42. M. BenSalah, R. Sabot, E. Triki, L. Dhouibi, Ph. Refait, M. Jeannin, *Corros. Sci.*, 86 (2014) 61.
43. L.V. Taveira, M.F. Montemor, M. Da Cunha Belo, M.G. Ferreira, L.F.P. Dick, *Corros. Sci.*, 52 (2010) 2813.
44. Yazhou Zhao, Tao Pan, Xiaotong Yu, Da Chen, *Corros. Sci.*, 158 (2019) 108097.
45. Jin-Ju Park, Su-Il Pyun, *Corros. Sci.*, 46 (2004) 285.
46. Miranda, Jesualdo Pereira Farias, Luciano Andrei Bergmann, Jorge F. dos Santos, *J. Mater. Res. Technol.*, 8 (2019) 1878.
47. Y.Y. Li, Z.Z. Wang, X.P. Guo, G.A. Zhang, *Corros. Sci.*, 147 (2019) 260.
48. Xiangfeng Zhang, Jun Wang, Hongyuan Fan, Dong Pan, *Appl. Surf. Sci.*, 440 (2018) 755.
49. Decheng Kong, Chaofang Dong, Xiaoqing Ni, Liang Zhang, Jizheng Yao, Cheng Man, Xuequn Cheng, Kui Xiao, Xiaogang Li, *J. Mater. Sci. Technol.*, 35 (2019) 1499. .
50. Sicong Shen, Xiaolong Song, Qizhen Li, Xinfeng Li, Ruihua Zhu, Gongxian Yang, *Mat. Sci. Eng.A.*, 740-741 (2019) 243.
51. Mirosław Szala, Karolina Beer-Lech, Mariusz Walczak, *Eng. Fail. Anal.*, 77 (2017) 31.